Determination of absolute photoionization cross sections of the phenyl radical

Niels E. Sveum,[ab] Scott J. Goncher[ab] and Daniel M. Neumark*[ab]

Received 3rd October 2005, Accepted 5th December 2005
First published as an Advance Article on the web 20th December 2005
DOI: 10.1039/b513960k

Photoionization cross sections of the phenyl radical to form the phenyl cation were measured using tunable vacuum ultraviolet synchrotron radiation coupled with photofragment translational spectroscopy. The phenyl radical was produced *via* 193- or 248-nm dissociation of chlorobenzene. At 10.0 eV, the photoionization cross sections for the phenyl radical averaged over product channels were found to be 13.4 ± 2.0 and 13.2 ± 2.0 Mb, respectively, with very little effect seen from the range of internal excitation produced at the two photolysis wavelengths. Using the photoionization cross section values for each channel, photoionization efficiency curves for the phenyl radical were placed on an absolute scale from 7.8 to 10.8 eV.

Introduction

The development of intense vacuum ultraviolet (VUV) light sources, including synchrotrons and VUV lasers, has substantially expanded the role of VUV light in physical chemistry experiments, ranging from photodissociation and molecular beam scattering to flame diagnostics.[1–7] These experiments utilize VUV radiation to photoionize reaction or photoproducts, which in turn are mass-selected and detected. Photoionization (PI) aids in product identification and characterization because it yields substantially less fragmentation upon ionization as compared to detection schemes based on electron impact ionization. However, extraction of information such as product branching ratios from photoionization experiments requires PI cross sections for all chemical species probed. While PI cross sections of several closed shell molecules have been determined,[8] determining these cross sections for radicals is quite challenging; it is generally difficult to produce known concentrations of these species, although some progress in this area has been made using cavity ringdown spectroscopy.[9]

Recently, our research group demonstrated a general approach to obtaining PI cross sections for radicals.[10,11] Photofragment translational spectroscopy (PTS)[12] is coupled with tunable VUV-PI of a pair of momentum-matched photofragments, one of which has a known PI cross section, to determine the PI cross section of the radical of interest. This technique yields the radical PI cross section, even when the system exhibits complex dissociation dynamics. Here, we investigate the phenyl radical (C_6H_5), produced *via* 193- and 248-nm photolysis of chlorobenzene with a goal of determining its absolute PI cross sections using the known PI cross section for atomic chlorine[8,13–16] for the two production methods.

The phenyl radical plays an important role in combustion chemistry. It can undergo either oxidation or polymerization reactions, with the latter leading to formation of polyaromatic hydrocarbons (PAHs) and, eventually, to soot.[17–19] PAH formation is also of interest to microwave spectroscopists and astrophysicists as these species are possible components of interstellar space.[20] Therefore the determination of the absolute PI cross section of phenyl radical would be quite useful, most specifically in the analysis of organic flames and soot formation processes. An additional goal of this study is to explore the effects of internal excitation on the absolute PI cross section on a free radical. The internal energy of the radical fragment is a possible issue in our measurements because no cooling of the radical occurs after its creation through the dissociation of the precursor molecule. We can vary the internal energy of the phenyl radical by using two different photolysis wavelengths to create the radical and taking advantage of the multiple channels for chlorobenzene photodissociation that produce phenyl radicals with different internal energy distributions.

The photodissociation dynamics of chlorobenzene have been studied at 248 nm[21] and 193 nm[22,23] using molecular beam photofragment translational spectroscopy. In each study, only the recoiling chlorine fragment was monitored, and center-of-mass (CM) frame translational energy distributions ($P(E_T)$ distributions) were derived that fit this photoproduct. From these experiments, it was concluded that 193-nm excitation of chlorobenzene results in three distinct dissociation channels resulting from C–Cl bond fission. The fastest products were attributed to a direct dissociation or fast predissociation, the second channel to dissociation from vibrationally excited triplet levels, and the slowest products to internal conversion followed by dissociation from highly excited vibrational levels of the ground electronic state. Photodissociation at 248 nm was proposed to occur *via* the second and third channels only.

The interpretation of these experiments was supported in recent theoretical work of Lunell and co-workers[24,25] This theoretical analysis also yielded state labels for the origin of the observed dynamics. Fig. 1 illustrates the diabatic potential-energy curves along the Cl–C_6H_5 bond of chlorobenzene, as

[a] *Department of Chemistry, University of California, Berkeley, CA 94720, USA. E-mail: dneumark@berkeley.edu*
[b] *Chemical Sciences Division, Lawrence Berkeley National Laboratory, Berkeley, CA 94720, USA*

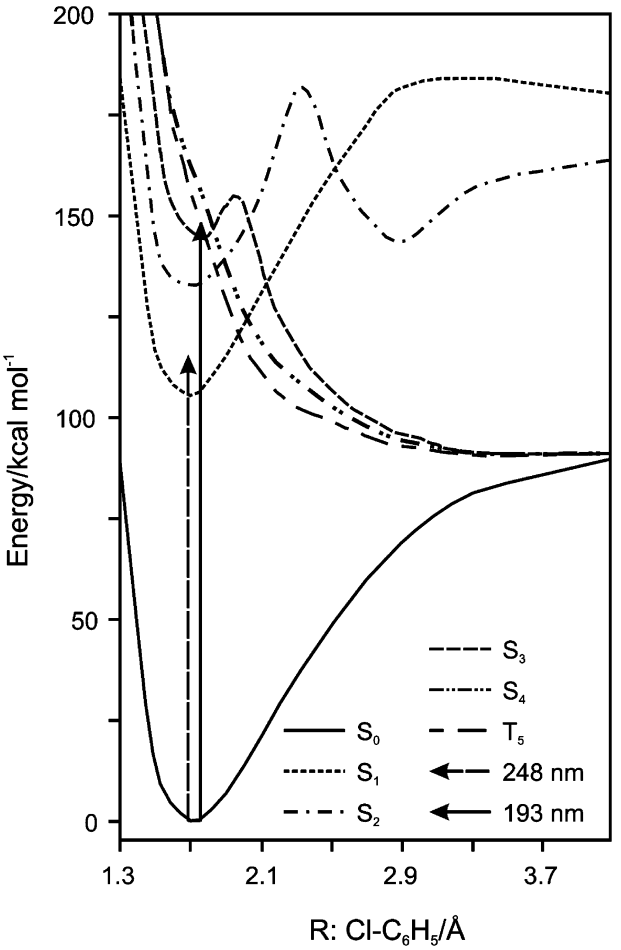

Fig. 1 Potential energy curves along the Cl–C_6H_5 bond of chlorobenzene adapted from ref. 25. The arrows indicate the 248- and 193-nm excitation energy used in the experiments.

determined by Lunell's group, that are of interest with respect to 193- and 248-nm photolysis. At 193 nm, the fastest photoproducts result from a direct dissociation to the repulsive (n,σ*) S_4 state or predissociation *via* tunneling from the quasibound (π,π*) S_3 state. The second channel is attributed to an intersystem crossing from the (π,π*) S_3 state to the repulsive (n,σ*) T_5 state. The slowest channel takes place *via* high vibrational levels of the ground S_0 state, populated by sequential internal conversion processes $S_3 \rightarrow (\pi,\pi^*)S_1 \rightarrow S_0$. At 248 nm, the fast fragments result from an intersystem crossing from the quasibound S_1 state to the repulsive (n,σ*) T_5 state or internal conversion from the S_1 state to the repulsive S_4 state. The slow products come from internal conversion from the S_1 state to the ground S_0 state, producing highly vibrationally excited molecules with enough energy to dissociate.

In this paper, we investigate the photodissociation dynamics of chlorobenzene in more detail at 248 and 193 nm. The complexity of the photodissociation dynamics of chlorobenzene provides a stringent test of our method for measuring the photoionization cross section of the phenyl radical, in particular the dependence of the cross section upon internal energy of the radical. The multiple dissociation channels at the two photolysis wavelengths used in this study result in phenyl production with a wide variation in internal energy. Nonetheless, we find relatively little variation of the photoionization cross section of the radical over the energy range studied here (7.8–10.8 eV).

Experiment

The experiments described in this paper are performed using a rotating source/fixed detector crossed molecular beams instrument located on the Chemical Dynamics Beamline at the Advanced Light Source. This instrument has been described in detail previously[1] and is configured for PTS measurements. Briefly, a pulsed molecular beam of ~5.0% chlorobenzene (99.9% Aldrich) seeded in helium is formed by means of a pulsed valve (400 Hz, 0.5 mm diameter nozzle, 300 Torr) heated to 100 °C. The molecular beam is skimmed and intersected by either a 193 nm ArF or 248 nm KrF excimer laser beam, which is unpolarized, propagating orthogonally to both the molecular beam and the detector axes. In this configuration, the photofragment angular distribution is isotropic in the plane of detection. The laser beam is focused to 8 mm^2 and the laser power is maintained at ~11 mJ $pulse^{-1}$ to minimize multiphoton processes.

Scattered photoproducts accepted by the detector travel 15.1 cm prior to ionization by tunable VUV synchrotron radiation. They are mass-selected by a quadrupole mass filter and counted as a function of time with a multichannel scaler, producing angle-resolved time of flight (TOF) spectra for the ions of a specific mass-to-charge ratio (m/e). Properties of the VUV radiation have been described elsewhere.[26] A rare gas filter is utilized to remove the higher harmonics of the undulator radiation[26] and a MgF_2 window is positioned in the path of the undulator radiation for PI energies below 11.0 eV to mitigate the effects of any residual high energy tail on the fundamental. The energy resolution ($\Delta E/E$) of the radiation is 2.3%.

As in previous studies[10,11] two types of photodissociation measurements are performed. First, a set of laboratory-frame TOF spectra for Cl and phenyl photofragments at several laboratory angles (Θ_{LAB}) is collected at VUV photon energies of 15.0 and 10.0 eV for the two fragments, respectively. Analysis of these spectra yields CM-frame $P(E_T)$ distributions for each process and the PI cross section for the phenyl radical at 10 eV. Second, a series of TOF spectra for the phenyl radical is obtained by stepping the undulator radiation while remaining at a fixed Θ_{LAB} (30°) and m/e. Integrating this set of measurements followed by normalization yields a photoionization efficiency (PIE) curve, which is put on an absolute scale by means of the PI cross section determination at 10 eV.

Results and analysis

TOF spectra were taken for several laboratory angles ranging from 10 to 60° for both atomic chlorine (m/e = 35) and phenyl radical (m/e = 77). Fig. 2 illustrates representative TOF spectra for m/e = 35 and 77 at Θ_{LAB} = 30° produced by the photodissociation of chlorobenzene at 193 and 248 nm;

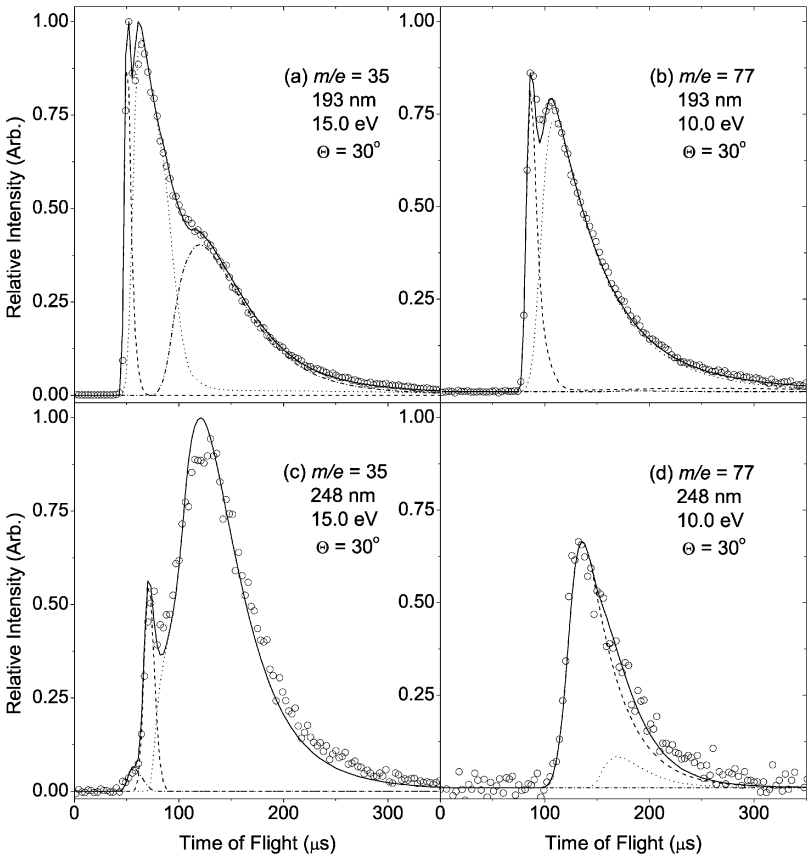

Fig. 2 TOF spectra from chlorobenzene dissociation: (a) $m/e = 35$ (Cl^+) and (b) $m/e = 77$ ($C_6H_5^+$) at $\Theta_{LAB} = 30°$ from 193-nm dissociation; (c) $m/e = 35$ (Cl^+) and (d) $m/e = 77$ ($C_6H_5^+$) at $\Theta_{LAB} = 30°$ from 248-nm dissociation. TOF signal has been normalized for laser shots, laser power, VUV photon flux, and isotopic abundance. The $m/e = 77$ signal has been normalized with respect to the $m/e = 35$ signal for each pair. The open circles represent the data and the solid line represents the total forward convolution fit to the data. For (a) and (b) the $P(E_T)$ distributions from Fig. 3 are used to fit the data. The $P(E_T)$ distributions from Fig. 4 are used to fit the data in (c) and (d). Dashed lines are from the distributions in Fig. 3a and 4a, dotted lines are from Fig. 3b and 4b, and the dashed-dot lines in Fig. 2a and 2b are from Fig. 3c. The fast dashed-dot feature in Fig. 2c is from a small multiphoton contribution.

VUV photoionization energies are indicated in the figure. For $m/e = 35$, a PI energy of 15.0 eV without the MgF_2 window is employed. The open circles in Fig. 2 represent the data points, while the solid line is the total fit to the data, generated by the procedure outlined below. The TOF spectra clearly comprise multiple contributions. At 193 nm, the spectrum for $m/e = 35$ shows two relatively fast peaks with a broad shoulder at longer arrival time, while at 248 nm, $m/e = 35$, one observes partially resolved fast and slow peaks. Hence there appear to be three distinct channels at 193 nm, and two at 248 nm, in agreement with previous work[21–23].

Fits to the TOF spectra are obtained by forward convolution of center-of-mass $P(E_T)$ distribution(s), with various parameters that characterize the instrument.[27,28] Based on the appearance of the TOF spectra, three $P(E_T)$ distributions were used to fit the data at 193 nm, and two at 248 nm. Each $P(E_T)$ distribution was adjusted point-wise until the simulated TOF spectra simultaneously fit the measured TOF spectra at all observed angles. In each case, the total fit is the sum of the fits from the individual dissociation channels, each of which is represented by a partial line in Fig. 2. At each photolysis wavelength, all TOF spectra for the $m/e = 35$ and 77 products were fit with the same set of $P(E_T)$ distributions, indicating the fragments are momentum-matched and that no appreciable secondary dissociation of the phenyl radical occurs for any of the dissociation channels.

The three $P(E_T)$ distributions in Fig. 3 fit the TOF spectra from 193-nm photolysis, while the two $P(E_T)$ distributions in Fig. 4 fit the data at 248 nm. Each channel is differentiated by the partitioning of the available energy between translation and internal excitation. Fig. 3a shows the distribution with the highest translational energy, while Fig. 3b and 3c have progressively less translational energy. The fast and slow distributions that fit the data at 248 nm are shown in Fig. 4a and 4b, respectively. Table 1 summarizes the characteristics of each $P(E_T)$ distribution in Figs. 3 and 4. Our $P(E_T)$ distributions for the various dissociation components at the two wavelengths are similar but not identical to those reported by Ichimura *et al.*;[21] our distributions peak at similar values of translational energy but are in general narrower. These differences are not surprising given that we can more cleanly resolve the individual contributions to the total photodissociation signal.

As described in our previous studies,[10,11] the PI cross sections for the unknown species (*i.e.* the phenyl radical) are

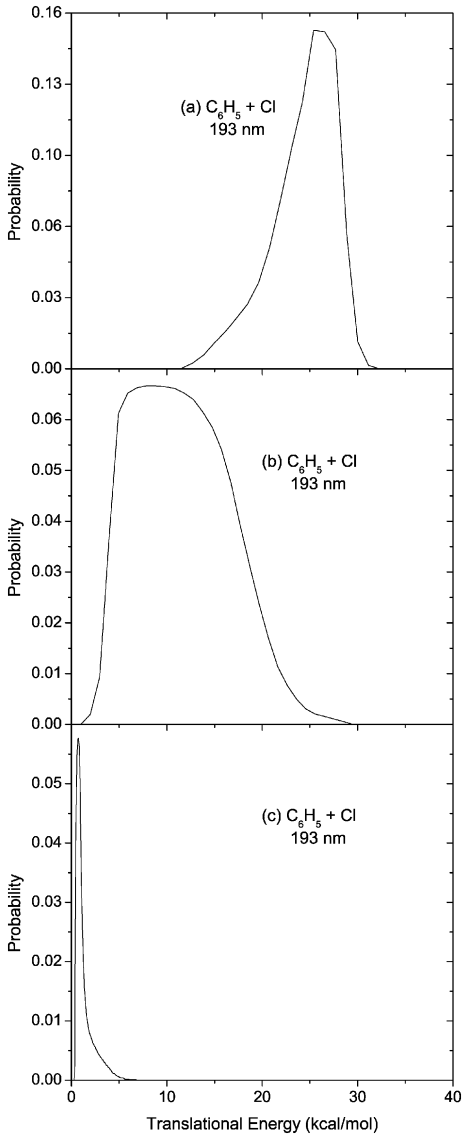

Fig. 3 $P(E_T)$ distributions for C_6H_5 + Cl from chlorobenzene at 193 nm. Three components are observed, characterized by a fast (a), a medium (b) and a slow (c) $P(E_T)$ distribution. Values of these point-wise distributions are specified every 1.0 kcal mol^{-1}.

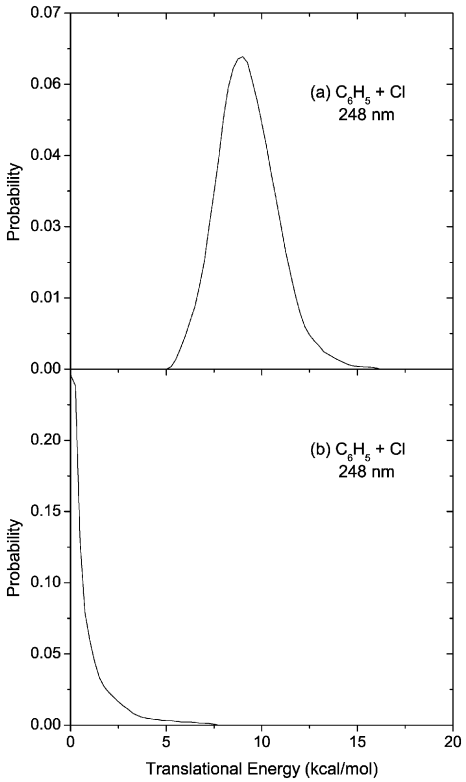

Fig. 4 $P(E_T)$ distributions for C_6H_5 + Cl from chlorobenzene at 248 nm. Two components are observed characterized by a fast (a) and a slow (b) $P(E_T)$ distribution. Values of these point-wise distributions are specified every 0.25 kcal mol^{-1}.

obtained by determining scaling factors for the $P(E_T)$ distributions in Fig. 3 and 4 needed to fit the relative intensities of the TOF data for the two product species. These scaling factors represent the ratio of weighting factors necessary for the convolution of the $P(E_T)$ distribution to reproduce the observed laboratory frame TOF intensities, while accounting for all the kinematic effects. The relative photoionization cross section for the momentum-matched photofragments, from $C_6H_5Cl + h\nu_{193\ nm}/h\nu_{248\ nm} \rightarrow C_6H_5 + Cl$, is obtained at specific PI energies ($\sigma_{C_6H_5}$[10 eV]/σ_{Cl}[15 eV]). The relative PI cross sections are normalized for experimental conditions such as laser power, number of laser shots, VUV photon flux and isotopic abundance. The difference in quadrupole transmission for the two ion masses is expected to be small, as discussed previously,[4] and is neglected in our analysis. Once σ_{Cl}[15 eV] is known, we can obtain $\sigma_{C_6H_5}$[10 eV]. Moreover, we apply this procedure to the momentum-matched photofragments associated with each of the five channels in Fig. 3 and 4, thereby testing the effect of internal energy of the phenyl radical on its photoionization cross section.

Table 1 Relevant quantities from CM translational energy distributions used to fit the laboratory frame data including the average translational energy ($\langle E_T \rangle$), the maximum available energy for each channel (E_{avl}), the maximum value of E_T in the distribution ($E_{T,max}$), the average internal energy (E_I) and the PI cross section of the phenyl radical at 10.0 eV ($\sigma_{10\ eV}$)[a]

Channel	Figure	$\langle E_T \rangle$	E_{avl}	$E_{T,max}$	E_I	$\sigma_{10\ eV}$
193 nm: Fast	3a	26.7	51.1	42.6	24.4	13.2
193 nm: Med	3b	12.6	51.1	26.5	38.5	12.9
193 nm: Slow	3c	2.1	51.1	10.9	49.0	14.0
248 nm: Fast	4a	9.2	18.3	16.0	9.1	13.9
248 nm: Slow	4b	1.1	18.3	8.6	17.2	13.2

[a] All values are in units of kcal mol^{-1} except cross section, which is in units of Mb.

The photoionization energy for Cl, 15 eV, lies between the thresholds for ionization to the Cl^+ $^1D_2$ and $^1S_0$ states. Although there is significant autoionization structure between these two thresholds, the selected photon energy is at the center of a very flat region (about 0.7 eV wide) in the photoionization efficiency curve for Cl, as measured by Ruscic and Berkowitz.[13] In their paper, the PIE curve for Cl was placed on an absolute basis by comparison with several many-body calculations, yielding σ_{Cl}[15 eV] as 31 Mb. However, in more recent work, Berkowitz[8] recommends setting σ_{Cl} to 34.2 Mb at the $Cl^+(^1S)$ edge (16.42 eV),[13] based upon analysis of multiple experimental and theoretical studies. Using this value, appropriate scaling of the PIE curve yields σ_{Cl}[15 eV] = 27.3 Mb. With this value for σ_{Cl}[15 eV], we then obtain $\sigma_{C_6H_5}$[10 eV]. Although Berkowitz gives no error bars for σ_{Cl}, his discussion of other experimental and theoretical values of the cross section at 16.42 eV suggests a conservative estimate of ±10%. This uncertainty, combined with other smaller factors (mainly the quadrupole transmission function), leads us to assign error bars of ±15% for our absolute cross sections.

Table 1 lists the resulting absolute PI cross sections $\sigma_{C_6H_5}$ [10 eV], for the phenyl radical associated with each $P(E_T)$ distribution in Fig. 3 and 4. The range of values is quite narrow, from 12.9 to 14.0 Mb, and there is no obvious correlation with photofragment internal energy; at 193 nm, the slowest fragments have the highest cross section, but the opposite trend is seen at 248 nm. The cross sections at each wavelength averaged over all observed photodissociation channels (including all relative weighting factors) are 13.4 ± 2.0 and 13.2 ± 2.0 Mb at 193 and 248 nm, respectively.

The narrow range of values for $\sigma_{C_6H_5}$[10 eV] is important for another reason. The value of σ_{Cl}[15 eV] used in our analysis applies only to the $Cl(^2P_{3/2})$ state. No experimental or theoretical results are available for the $Cl^*(^2P_{1/2})$ state, which lies about 0.1 eV above the $Cl(^2P_{3/2})$ state. The $Cl^*(^2P_{1/2})$ state could be produced in our experiment, but we do not have the means to distinguish it from the $Cl(^2P_{3/2})$ state, since the spin–orbit splitting is less than the bandwidth of the VUV radiation. Assuming the Cl* channel to be non-negligible, one would expect the five photodissociation channels investigated in our experiment to produce different spin–orbit populations of the Cl atoms, given that multiple electronic states are involved in the various channels. Under these circumstances, if the cross sections at 15 eV for the two states were very different, there would be significant variations in the phenyl cross sections extracted from our analysis. Instead, all five values listed in Table 1 lie within the 15% error bars associated with our selected value of σ_{Cl}[15 eV], suggesting that the production of spin–orbit excited chlorine has a very small effect on the phenyl PI cross sections. Hence, it would appear that either the cross sections for Cl and Cl* at 15 eV are similar, or that none of the five channels involve significant production of Cl*.

PIE curves for C_6H_5 photoproducts were determined for the three channels at 193 nm and the two at 248 nm by fitting the contribution from each channel to the TOF distribution at a series of VUV photon energies. The five resulting curves are placed on an absolute scale using the cross sections at 10.0 eV as illustrated in Fig. 5. At PI energies above 9.4 eV, all the curves are very comparable albeit with a bit of spread, until the cross section drops off a bit above 10.6 eV. However, for PI energies below 9.2 eV, the C_6H_5 fragments produced *via* 193-nm photolysis, which have more internal energy, demonstrate a slightly higher cross section than those produced from 248-nm photolysis. None of the curves show much signal below the ionization potential of the phenyl radical, for which values of 8.1 and 8.3 eV have been reported by photoionization mass spectrometry[29] and photoelectron spectroscopy,[30] respec-

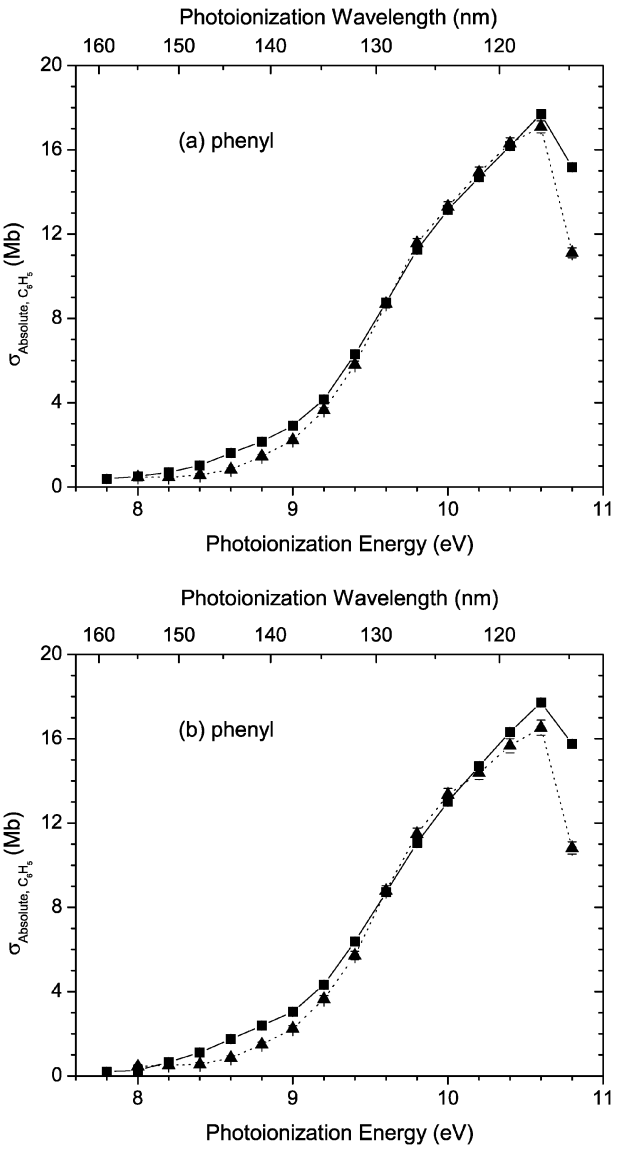

Fig. 5 PIE curves for m/e = 77 ($C_6H_5^+$) photoproduct at Θ_{LAB} = 30° using the MgF_2 window. (a) Photofragments resulting from 193-nm photolysis, where the squares represent fragments with the $P(E_T)$ distribution shown in Fig. 3a, the triangles are for products with the $P(E_T)$ distribution shown in Fig. 3b and the circles signify photofragments with the $P(E_T)$ distribution shown in Fig. 3c. (b) Photoproducts from 248-nm dissociation, where the squares are for products with the $P(E_T)$ distribution from Fig. 4a and the triangles are for the products with the $P(E_T)$ distribution shown in Fig. 4b.

tively. Overall, all five PIE curves are quite similar, considering that the average internal energy of the photofragments ranges from 9 to nearly 50 kcal mol^{-1} (Table 1).

Discussion

By analyzing the photodissociation of chlorobenzene with a rotating source crossed molecular beam machine, this experiment has been able to provide a more detailed experimental study of the dynamics associated with C–Cl bond fission. The $P(E_T)$ distributions presented here should be more accurate than those reported previously,[21–23] in that they fit the data for momentum-matched fragments at many laboratory angles simultaneously, while those of previous studies only fit a single laboratory angle. However, our results support the mechanisms inferred from previous experimental and theoretical work[24,25] as described in the Introduction.

In addition to being able to probe the dynamics of the dissociation event, this experiment allows for the absolute PI cross section of the phenyl radical to be determined. The chlorobenzene system provides a unique opportunity to not only measure the absolute PI cross section of the phenyl radical, but also to investigate the effects of internal excitation on the PI cross section. This issue is important in our experiments because polyatomic photoproducts do not undergo any collisions following the photolysis of chlorobenzene, so no relaxation of the internal excitation as determined by the photodissociation dynamics can occur. However, neither the cross sections at 10 eV nor the PIE curves show much dependence on the internal energy.

These results are of interest in light of past studies of the photoionization of the phenyl radical. The phenyl cation has two low-lying states, a $^1A_1$ state and $^3B_1$ state, formed by removal of a σ and π electron, respectively, from the $^2A_1$ ground state of the phenyl radical.[31] Electronic structure calculations on the cation generally agree that the $^1A_1$ is lower in energy by less than 1 eV, but that the geometry change upon photoionization is much larger to the $^1A_1$ state than to the $^3B_1$ state.[30–34] As a result, Butcher *et al.*[30] assigned their photoelectron spectrum of the phenyl radical to transitions to the triplet state, because the expected Franck–Condon profile was expected to be so extended that it would be very difficult to observe in the photoelectron spectrum. The most recent calculations, by Hrusak *et al.*,[33] find adiabatic IP's of 8.07 and 8.87 eV to the $^1A_1$ and $^3B_1$ states, respectively. Hrusak *et al.* simulated the phenyl photoelectron spectrum, assuming the partial cross sections for the two ionization channels were the same. They found the triplet band to be quite compact and dominated by the vibrational origin transition, while the singlet band is spread out over several eV, thus supporting the assignment by Butcher *et al.*[30]

The insensitivity of the PIE curves in Fig. 5 to the internal energy of the C_6H_5 product is consistent with photoionization to the triplet state of the cation as the major channel in this energy region. The relatively small geometry change upon photoionization to the triplet state implies that diagonal ($\Delta v = 0$) vibrational transitions are favored, minimizing the effect of vibrational excitation in the radical on the PIE curves. The larger signal in the region of the IP for 193-nm photolysis is the most prominent effect of higher internal energy, and most likely does reflect photoionization from vibrationally excited levels of the radical, but overall, these effects appear to be quite small. Our absolute PI cross sections above 9.0 eV are thus expected to be intrinsic properties of the phenyl radical as opposed to values that are strongly dependent on its method of preparation. It will be of interest to investigate the cross sections of radicals for which larger geometry changes are expected to occur upon photoionization to gain further insight into the robustness of the values obtained from our experiment.

Conclusions

PTS has been coupled with VUV-PI detection in order to determine the PI cross sections for the phenyl radical generated *via* 193- and 248-nm dissociation of chlorobenzene. Despite the complex dynamics associated with the photodissociation of chlorobenzene, the relevant PI cross sections can be extracted by fitting momentum-matched TOF data from the Cl and C_6H_5 photofragments. At 10.0 eV, the cross sections for the high, medium and low translational energy photoproducts from 193-nm dissociation are found to be 13.2, 12.9, and 14.0 Mb, respectively. Similarly for 248-nm dissociation, the cross sections at 10.0 eV are 13.9 Mb for fragments with high translational energy and 13.2 Mb for products with low translation energy. All values have error bars of $\pm 15\%$. These cross sections are used to place the PIE curves for the C_6H_5 photofragments on an absolute scale from 7.8 to 10.8 eV. The small variation of the PI cross sections and PIE curves with phenyl radical internal energy bodes well for future measurements using this technique.

Acknowledgements

This work was supported by the Director, Office of Basic Energy Sciences, Chemical Sciences Division of the US Department of Energy under contract No. DE-AC02-05CH11231.

References

1 X. Yang, J. Lin, Y. T. Lee, D. A. Blank, A. G. Suits and A. M. Wodtke, *Rev. Sci. Instrum.*, 1997, **68**, 3317.
2 J. A. Mueller, B. F. Parsons, L. J. Butler, F. Qi, O. Sorkhabi and A. G. Suits, *J. Chem. Phys.*, 2001, **114**, 4505.
3 J. C. Robinson, W. Z. Sun, S. A. Harris, F. Qi and D. M. Neumark, *J. Chem. Phys.*, 2001, **115**, 8359.
4 J. C. Robinson, S. A. Harris, W. Z. Sun, N. E. Sveum and D. M. Neumark, *J. Am. Chem. Soc.*, 2002, **124**, 10211.
5 W. S. McGivern, O. Sorkhabi, A. G. Suits, A. Derecskei-Kovacs and S. W. North, *J. Phys. Chem. A*, 2000, **104**, 10085.
6 T. A. Cool, K. Nakajima, T. A. Mostefaoui, F. Qi, A. McIlroy, P. R. Westmoreland, M. E. Law, L. Poisson, D. S. Peterka and M. Ahmed, *J. Chem. Phys.*, 2003, **119**, 8356.
7 C. A. Taatjes, N. Hansen, A. McIlroy, J. A. Miller, J. P. Senosiain, S. J. Klippenstein, F. Qi, L. S. Sheng, Y. W. Zhang, T. A. Cool, J. Wang, P. R. Westmoreland, M. E. Law, T. Kasper and K. Kohse-Hoinghaus, *Science*, 2005, **308**, 1887.
8 J. Berkowitz, *Atomic and Molecular Photoabsorption Absolute Total Cross Sections*, Academic Press, San Diego, CA, 2002.
9 J. J. Scherer and D. J. Rakestraw, *Chem. Phys. Lett.*, 1997, **265**, 169.

10 J. C. Robinson, N. E. Sveum and D. M. Neumark, *J. Chem. Phys.*, 2003, **119**, 5311.
11 J. C. Robinson, N. E. Sveum and D. M. Neumark, *Chem. Phys. Lett.*, 2004, **383**, 601.
12 L. J. Butler and D. M. Neumark, *J. Phys. Chem.*, 1996, **100**, 12801.
13 B. Ruscic and J. Berkowitz, *Phys. Rev. Lett.*, 1983, **50**, 675.
14 J. A. R. Samson, Y. Shefer and G. C. Angel, *Phys. Rev. Lett.*, 1986, **56**, 2020.
15 W. J. van der Meer, R. J. Butselaar and C. A. de Lange, *Aust. J. Phys.*, 1986, **39**, 779.
16 R. Flesch, J. Plenge, S. Kuhl, M. Klusmann and E. Ruhl, *J. Chem. Phys.*, 2002, **117**, 9663.
17 I. Glassman, *Combustion*, Academic Press, New York, 2nd edn, 1986.
18 B. V. Unterreiner, M. Sierka and R. Ahlrichs, *Phys. Chem. Chem. Phys.*, 2004, **6**, 4377.
19 I. V. Tokmakov, G. S. Kim, V. V. Kislov, A. M. Mebel and M. C. Lin, *J. Phys. Chem. A*, 2005, **109**, 6114.
20 E. Herbst, *Annu. Rev. Phys. Chem.*, 1995, **46**, 27.
21 T. Ichimura, Y. Mori, H. Shinohara and N. Nishi, *Chem. Phys.*, 1994, **189**, 117.
22 T. Ichimura, Y. Mori, H. Shinohara and N. Nishi, *Chem. Phys. Lett.*, 1985, **122**, 51.
23 A. Freedman, S. C. Yang, M. Kawasaki and R. Bersohn, *J. Chem. Phys.*, 1980, **72**, 1028.
24 Y. J. Liu, P. Persson and S. Lunell, *J. Phys. Chem. A*, 2004, **108**, 2339.
25 Y. J. Liu, P. Persson and S. Lunell, *J. Chem. Phys.*, 2004, **121**, 11000.
26 A. G. Suits, P. Heimann, X. M. Yang, M. Evans, C. W. Hsu, K. T. Lu, Y. T. Lee and A. H. Kung, *Rev. Sci. Instrum.*, 1995, **66**, 4841.
27 X. S. Zhao, PhD thesis, University of California, 1988.
28 J. D. Myers, PhD thesis, University of California, 1993.
29 Y. L. Sergeev, F. I. Vilesov and M. E. Akopyan, *Opt. Spektrosk.*, 1972, **32**, 230.
30 V. Butcher, M. L. Costa, J. M. Dyke, A. R. Ellis and A. Morris, *Chem. Phys.*, 1987, **115**, 261.
31 J. D. Dill, P. V. R. Schleyer, J. S. Binkley, R. Seeger, J. A. Pople and E. Haselbach, *J. Am. Chem. Soc.*, 1976, **98**, 5428.
32 A. Nicolaides, D. M. Smith, F. Jensen and L. Radom, *J. Am. Chem. Soc.*, 1997, **119**, 8083.
33 J. Hrusak, D. Schroder and S. Iwata, *J. Chem. Phys.*, 1997, **106**, 7541.
34 F. Bernardi, F. Grandinetti, A. Guarino and M. A. Robb, *Chem. Phys. Lett.*, 1988, **153**, 309.

